

PAPER

Effects of laser polarization and wavelength on hybrid laser wakefield and direct acceleration

To cite this article: Xi Zhang *et al* 2018 *Plasma Phys. Control. Fusion* **60** 105002

View the [article online](#) for updates and enhancements.




IOP | ebooks™

Bringing you innovative digital publishing with leading voices to create your essential collection of books in STEM research.

Start exploring the collection - download the first chapter of every title for free.

Effects of laser polarization and wavelength on hybrid laser wakefield and direct acceleration

Xi Zhang^{1,2}, T Wang² , V N Khudik^{1,2}, A C Bernstein¹, M C Downer¹ and G Shvets^{1,2,3}

¹Department of Physics and Institute for Fusion Studies, The University of Texas at Austin, Austin, TX 78712, United States of America

²School of Applied and Engineering Physics, Cornell University, Ithaca, NY 14850, United States of America

E-mail: gs656@cornell.edu

Received 10 April 2018, revised 24 July 2018

Accepted for publication 1 August 2018

Published 17 August 2018



CrossMark

Abstract

We demonstrate that hybrid laser wakefield and direct acceleration can be significantly improved by using two laser pulses with different polarizations or frequencies. The improvement entails higher energy and charge of the accelerated electrons, as well as weaker sensitivity to the time delay between the leading (pump) pulse responsible for generating the wakefield, and the trailing laser pulse responsible for direct laser acceleration (DLA). When the two laser pulses have the same frequency, it is shown that it is advantageous to have their polarization states orthogonal to each other. A specific scenario of a frequency-doubled ($\lambda_{\text{DLA}} = \lambda_{\text{pump}}/2$) DLA laser pulse is also considered, and found to be an improvement over the single-frequency ($\lambda_{\text{DLA}} = \lambda_{\text{pump}}$) format.

Keywords: direct laser acceleration, laser wakefield, ionization injection

(Some figures may appear in colour only in the online journal)

1. Introduction

From their early beginnings as a speculative theoretical idea [1], laser-plasma acceleration has developed into one of the most exciting advanced accelerator techniques that has already lead to the production of monoenergetic electron beams [2–4], and is now pushing the energy frontier to multi-GeV scale [5–8] and beyond [9]. Laser-wakefield acceleration (LWFA) is presently the most mature mechanism in laser-plasma electron acceleration. Rapid advances in laser technology enabled high-power high-intensity short pulse lasers capable of accessing the so-called full plasma blow-out (‘bubble’) regime [10, 11]. Plasma electrons are fully blown out from the path of the laser pulse by its ponderomotive force $F_p \sim m_e c^2 \nabla a^2$ (where $a = eA_L/mc^2$ is the normalized vector potential), thereby creating the plasma bubble in its

wake. The plasma bubble regime is crucial for generating the high energy monoenergetic electron beams [2–4].

At the same time, other laser-plasma acceleration techniques have also been critically evaluated. One of the most promising among those techniques is the direct laser acceleration (DLA) approach, in which the laser electromagnetic field directly imparts energy to the electrons [12, 13]. DLA relies on the betatron resonance that occurs when the Doppler-shifted laser frequency $\langle \omega_l \rangle \equiv \omega_L(1 - \langle v_x \rangle/v_{\text{ph}})$ matches the l th harmonic of the electron’s betatron frequency $\omega_\beta = \omega_p/\sqrt{2\langle \gamma \rangle}$: $\langle \omega_l \rangle = l\omega_\beta$, where $l = 1, 3, 5, \dots$ is an odd number that corresponds to either fundamental ($l = 1$) or higher-order ($l > 1$) betatron resonance [14, 15]. Here $\langle v_x \rangle$ and $\langle \gamma \rangle$ are the time-averaged (over a betatron period) longitudinal velocity and relativistic factor of the accelerated electron; ω_L and v_{ph} are the frequency and the phase velocity of the laser field; $\omega_p = \sqrt{4\pi n e^2/m}$ is the electron plasma frequency.

³ Author to whom any correspondence should be addressed.

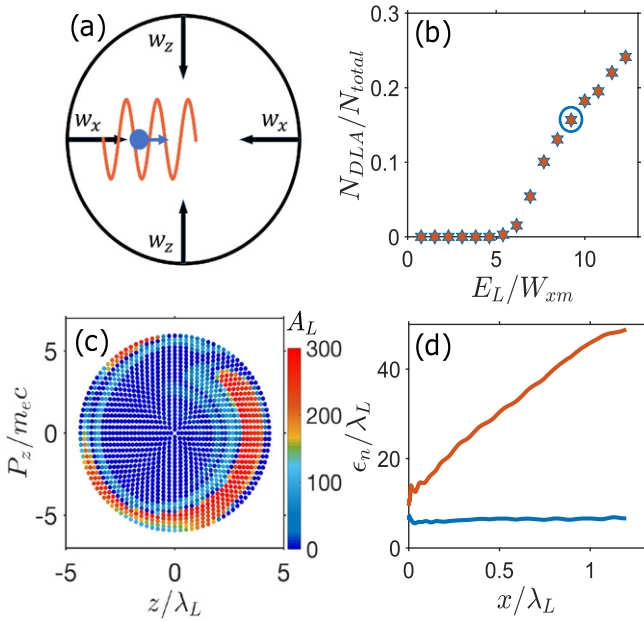


Figure 1. Single-particle dynamics governed by equations (1)–(3). (a) Schematic representation of single-particle simulation model. (b) The ratio between the number of DLA electrons N_{DLA} and the total number of accelerated electrons N_{total} as a function of the ratio between the laser and wake fields. The blue circle corresponds to the laser wave amplitude $E_L \approx 1.5mc\omega_L/e$ used in (c) and (d) simulations. (c) Color-coded energy gain A_L through the DLA mechanism as a function of the initial conditions in the transverse phase space (z, p_z) . (d) Evolution of the normalized emittance ϵ_n for the DLA (red line) and non-DLA (blue line) electrons.

Recently, the merger of the LWFA in the bubble regime and the DLA, which we refer to as the laser wakefield and direct acceleration (LWDA) mechanism, started attracting considerable attention because of the possibilities for producing high energy electron beams for high energy physics, as well as copious high-energy x-rays [16–31] for a variety of applications that require high-brightness radiation [32–36]. However, effective LWDA is not straightforward to achieve. Specifically, two requirements have been shown to be crucial for effective LWDA: (I) the initial energy $\epsilon_{\perp}(t=0)$ of betatron motion of an injected plasma electron must be sufficiently high to overcome its rapid reduction due to electron acceleration by the longitudinal field of the plasma bubble, (II) considerable overlap between the laser field and the injected electrons [16, 17, 19–23]. The first requirement is fulfilled by either density bump injection [16] or ionization injection [17–23, 31, 37, 38]. Both approaches can deliver an injected electron beam with the initial transverse energy sufficient for effective DLA.

One of the ways to meet the second requirement is to use the second (DLA) laser pulse time-delayed from the bubble-forming (pump) laser pulse [16, 17]. The two-pulse approach is even harder to implement using widely deployed [9, 11, 39–41] moderate-power (i.e. in the 10 TW range) laser pulses because they produce plasma bubbles of relatively small size. The combination of two equal-frequency laser pulses within a small bubble can result in undesirable interference between them, with two major consequences. First, the shape of the

plasma bubble can be strongly modified by the beatwave between the two pulses. As will be shown below, such modification can have a major effect on the total electron charge trapped inside the plasma bubble and subsequently accelerated by the combination of the LWFA and DLA mechanisms. Second, the peak laser field experienced by the injected electrons is also strongly modified by interference. This influences electrons' energy gain from the DLA mechanism, as well as the fraction of the injected electrons that experiences the DLA. The latter point will also be elaborated below.

From the above arguments we conclude that both the charge and the energy distribution of the accelerated electrons could become highly sensitive to the time delay $\Delta\tau$ between the two pulses. Therefore, eliminating the interference between them could make the LWDA scheme considerably more robust. There are two natural approaches to eliminating interference. One is to preserve the equal wavelengths of the two laser pulses ($\lambda_{DLA} = \lambda_{pump}$), but to make their polarization states mutually orthogonal. The orthogonal polarization of the pump and the DLA pulses can potentially rectify both of the above listed negative consequences of the interference between these two pulses. The other approach, the two-color laser pulse format, utilizes different wavelengths of the DLA and pump pulses: $\lambda_{DLA} < \lambda_{pump}$. Specifically, we will address the technologically viable scenario of $\lambda_{DLA} = \lambda_{pump}/2$. The advantage of such laser format can be understood from the $\propto\lambda^2$ scaling of the ponderomotive potential: the long-wavelength pump produces a large bubble while the short-wavelength DLA pulse does not perturb the bubble despite possessing a large electric field required to produce strong DLA.

Moreover, the duration and the spot size of the short-wavelength DLA pulse can be shortened as compared with the long-wavelength pump pulse, thus resulting in a higher or comparable pulse intensity for the same or smaller energy content. Finally, the disadvantageous $\propto\lambda^2$ scaling of the relativistic self-focusing power for the short-wavelength DLA pulse is not a concern because of its guiding by the bubble that was recently demonstrated in experiments and simulations [42]. We note that the advantage of combining low- and high-frequency laser pulses was suggested earlier [43–45] in a very different context of ionization injection. Guided by the technological considerations of the ease of doubling the laser frequency in a nonlinear crystal, we will explore the following combination of the laser wavelengths: $\lambda_{pump} = 0.8 \mu\text{m}$ for the pump laser pulse that produces the bubble and ionizes a high-Z gas, and $\lambda_{DLA} = 0.4 \mu\text{m}$ for the second time-delayed DLA laser pulse. The DLA pulse increases the energy gain of the electrons and enhances the charge yield without disturbing the plasma bubble. We also demonstrate the improved stability of the LWDA mechanism when the high-frequency DLA pulse is used.

The remainder of the paper is organized as follows. In section 2 we provide a review of the LWDA concept. Simplified single-particle simulations are used to illustrate some of the basic features of LWDA, such as the dependence of the number of DLA electrons on the laser amplitude. The

emittance growth of the beam composed of DLA electrons is also discussed. The comparison between different laser formats that can be used for LWDA is carried out in section 3 using first-principles 2D PIC simulations. The three different laser formats are: (a) single-color same-polarization LWDA, (b) single-color orthogonal polarization LWDA, and (c) two-color same-polarization LWDA. Here the color and polarization are the attributes of the pump and DLA pulses used for LWDA. Finally, we discuss the potential application of the DLA electron beam as a source of high-frequency betatron radiation. Conclusions and future research directions are outlined in section 5.

2. Review of LWDA principles using single-particle simulations

Figure 1(a) schematically illustrates the single-particle model. The nonlinear dynamics of relativistic electrons undulating in the (x, z) -plane is determined by the prescribed bubble wakefield and the electromagnetic field of the laser which is polarized in the undulation plane. Electrons are assumed to be moving in the combined fields of the moving spherical bubble, and of the laser pulse. The accelerating and focusing fields of the bubble are assumed in the following form [46]: $W_x = m\omega_p^2(x - r_b - v_b t)/2e$ and $W_z = m\omega_p^2 z/2e$, respectively, where r_b is the radius, and $v_b = c/(1 - \gamma_b^2)^{1/2}$ is the velocity of the bubble. The electric and magnetic fields of the linearly polarized laser pulse with frequency ω_L and phase velocity v_{ph} are assumed to be planar and given by the following expressions: $E_z^{(L)} = -E_L \sin \omega_L(t - x/v_{ph})$ and $B_y^{(L)} = B_L \sin \omega_L(t - x/v_{ph})$, where $B_L = cE_L/v_{ph}$. The resulting equations of motion [16, 17, 25, 29, 30] for individual electrons are as follows:

$$\frac{dx}{dt} = v_x = \frac{p_x}{m\gamma}, \quad \frac{dz}{dt} = v_z = \frac{p_z}{m\gamma}, \quad (1)$$

$$\frac{dp_x}{dt} = -e \left(W_x - \frac{v_z}{c} B_y^{(L)} \right) \quad (2)$$

$$\frac{dp_z}{dt} = -e \left(W_z + E_z^{(L)} + \frac{v_x}{c} B_y^{(L)} \right), \quad (3)$$

where $\gamma = (1 + \mathbf{p}^2/m^2c^2)^{1/2}$ is the electron relativistic factor.

In the simplified model, all laser and bubble parameters are assumed to be time-independent. To be specific, their following values were chosen: the bubble radius $r_b = 6\lambda_L$, its relativistic factor $\gamma_b = 10$, the laser wavelength $\lambda_L = 0.8 \mu\text{m}$. The ratio of the plasma and laser frequencies $\omega_p/\omega_L = 0.093$ was consistent with plasma density $n_0 = 1.5 \times 10^{19} \text{ cm}^{-3}$. The phase velocity of the laser light $v_{ph} = 1.0024c$ was approximated by the phase velocity of the lowest laser mode supported by the plasma channel as explained in the following [47]. Note that the used phase velocity is consistent with the one obtained by numerical measurements performed in our VLPL simulations. At the start of the simulation ($t = 0$), several thousand electrons are initialized near the bottom of the bubble. They are assigned identical longitudinal momenta

$p_x \approx \gamma_b mc$, but their transverse positions and momenta (z, p_z) are assigned so as to uniformly fill the phase space area $0 < \varepsilon_\perp \leq 1.7mc^2$, where $\varepsilon_\perp = p_z^2/2\gamma m + m\omega_p^2 z^2/4$ is the transverse energy [16, 17, 28, 46]. The maximum of the transverse energy $1.7mc^2$ corresponds to the maximum amplitude of betatron oscillations, which is limited by the bubble radius $4.5\lambda_L$ at the injection point. The z and p_z ranges (or bandwidths) are as follows: $|z| < 4.5\lambda_L$ and $|p_z| < 6mc$. The simulation is terminated when the electrons reach the bubble center. Note that, in this simplified model, the accelerated electrons overlap with the DLA pulse during the entire simulation because the laser pulse is assumed to be infinitely long.

We use the energy gain from the laser, $A_L = -e \int E_z^{(L)} v_z dt$, as a quantitative parameter separating the DLA and non-DLA electrons. Specifically, electrons are classified as belonging to the DLA fraction N_{DLA} if $A_L > 0.3\gamma_{\text{final}} mc^2$. Performing simulations for a wide range of laser intensities, we find that the number of electrons gaining energy through the DLA mechanism is insignificant when the laser electric field E_L is comparable to the accelerating wakefield W_x in the bubble (see figure 1(b) for the details). However, the fraction of the DLA electrons starts rapidly increasing with E_L as soon as $E_L/W_{xm} > 5$, where W_{xm} is the peak accelerating wakefield in the bubble. Based on the results presented in figure 1(b), we conclude that the yield of the DLA-accelerated charge in the LWDA scheme strongly depends on the amplitude of the laser. This explains why it may be necessary to use a second (DLA) laser pulse to strongly modify the total spectrum of the accelerated electrons, which includes the DLA and non-DLA fractions [16, 17]. Even for large laser wave amplitudes, only those electrons with large initial transverse energy are directly accelerated by the laser [16, 17, 28, 46]. It has been demonstrated that the electrons with such energies $\varepsilon_\perp(t = 0)$ can be produced by the density bump injection [16] or by the ionization injection [17, 31].

The specific case of $E_L/W_{xm} = 10$ (indicated in figure 1(b) by the blue circle) is examined in figures 1(c), (d). By plotting the laser energy gain A_L versus the initial electron position in the (z, p_z) -phase space (see figure 1(c)), we find that the DLA electrons can gain significant energy ($A_L > 200m_e c^2$) directly from the laser as long as their initial transverse energy satisfies the $0.7mc^2 < \varepsilon_\perp < 1.7mc^2$. Note that this condition can be met by either assigning a large initial off-axis displacement $z(t = 0)$, or a large initial transverse momentum $p_z(t = 0)$ to the electrons. This is consistent with the earlier finding that DLA electrons can be produced by either off-axis or off-peak ionization [17, 43, 44] of a high-Z gas: the former provides a large initial z whereas the latter provides a large initial p_z .

We further find that DLA is accompanied by considerable growth of the normalized emittance ϵ_n defined as

$$\epsilon_n = \langle p_x/m_e c \rangle \sqrt{\langle z^2 \rangle \langle (p_z/p_x)^2 \rangle - \langle zp_z/p_x \rangle^2}, \quad (4)$$

where $\langle \cdot \rangle$ denotes averaging over the electron ensemble. On the other hand, the emittance of the non-DLA electrons remains almost constant during acceleration process. These

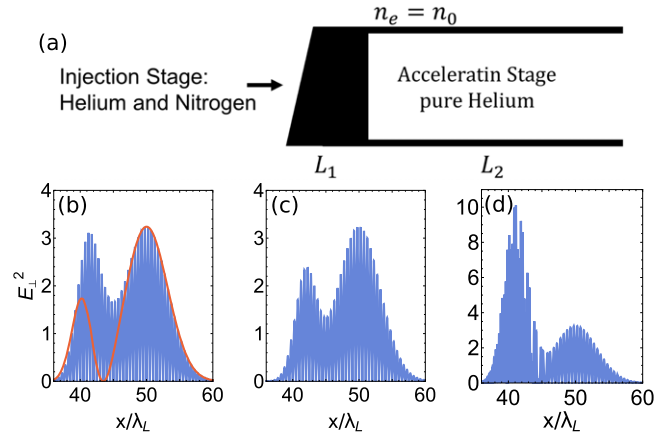


Figure 2. Schematic representation of the plasma density profile and the laser pulse formats. (a) The two-stage density profile: the injection stage (80%He + 20%N₂⁵⁺, $L_1 = 100 \mu\text{m}$) and acceleration stage (100%He, $L_2 \simeq 1 \text{ mm}$). Percentages are based on the electron density. (b) Initial on-axis intensity ($\propto E_{\perp}^2$) for the SP-LWDA case: $\lambda_{\text{DLA}} = \lambda_{\text{pump}} = \lambda_L$ and time delay $\Delta\tau = \delta\tau_0 = 24 \text{ fs}$. Red curve corresponds to the intensity profile for the time delay $\Delta\tau = \Delta\tau_0 + 0.5\lambda_L/c$. (c) Same as (b), but for the SO-LWDA case. (d) Same as (b), but for the TP-LWDA case: $2\lambda_{\text{DLA}} = \lambda_{\text{pump}} = \lambda_L$. In all cases E_{\perp} is normalized to $mc\omega_L/e$.

trends are illustrated in figure 1(d). As the red line, corresponding to the emittance growth of the DLA beam, indicates, the DLA electrons start with a larger emittance at $t = 0$, and further increase their emittance by a factor ≈ 5 . As we demonstrate below, this feature of the LWDA can be used for designing sources of intense x-ray betatron radiation. On the other hand, the emittance of the non-DLA starts small and remains such.

3. The effects of laser polarization and wavelength on DLA

In this section, we use self-consistent relativistic particle-in-cell (PIC) simulations to investigate the effects of polarization and color of laser pulses on LWDA. The simulations were carried out using 2D PIC code VLPL [48] with the implemented ADK tunneling ionization model [49–51] for the inner shell electrons. Note that the laser evolution, the trapping condition, and the energy gain from DLA differ between 2D and 3D simulations and therefore some differences are expected in the latter simulations.

The schematic and parameters of different proposed LWDA scenarios—single color parallel polarization LWDA (SP-LWDA), SO-LWDA and two color parallel polarization LWDA (TP-LWDA)—are shown in figure 2 and table 1. The entire interaction region is comprised of the injection and the acceleration stages. Both stages are assumed to contain easily-ionizable background helium gas. We assume that the background plasma of the density $n_0 = 1.5 \times 10^{19} \text{ cm}^{-3}$ is formed by the leading edge of the pump pulse that fully ionizes the helium gas and the outer shells of the nitrogen gas which is added to the short injection stage shown in

figure 2(a) as a dark area. The electrons are assumed to be injected into the plasma bubble through the process of tunneling ionization of high-Z nitrogen ions (N⁵⁺ and N⁶⁺) inside the injection stage. Such two-stage injection/acceleration schemes have been experimentally implemented [52, 53]. The sub-hundred micrometer gas nozzles that would be required to implement the injection stage for the design parameters of our simulations have also been experimentally realized [54, 55].

For our simulations, laser parameters (including its temporal profile) were chosen to be consistent with the UT³ laser system [11, 39]. For all three laser pulse formats we assumed that a two-pulse laser beam is formed by combining a 10 TW-class pump pulse ($P_{\text{pump}} = 12 \text{ TW}$) with the time-delayed DLA pulse ($P_{\text{DLA}} = 10 \text{ TW}$). Figures 2(b)–(d) shows the initial on-axis transverse laser electric field E_{\perp}^2 in different scenarios—SP-LWDA, SO-LWDA, and TP-LWDA. In all three scenarios, we keep the normalized vector potential a_{DLA} and the power P_{DLA} of the DLA laser pulses fixed. The reason for maintaining fixed a_{DLA} is primarily illustrative: it enables us to eliminate trivial differences between the plasma bubbles in these cases because those would arise from the difference in the ponderomotive pressure of the DLA pulse on the wall of the bubble. In the case of a TP-LWDA ($\lambda_{\text{DLA}} = 0.5\lambda_{\text{pump}}$), the constant a_{DLA} is maintained unchanged by using tighter focusing of the DLA pulse.

Our simulations indicate that the inner-shell nitrogen electrons (N⁵⁺ \rightarrow N⁶⁺ and N⁶⁺ \rightarrow N⁷⁺) are produced via tunneling ionization close to the peak of the pump pulse intensity. These electrons are then injected and trapped inside the plasma bubble [56–59]. At least some ionization can also be produced by the DLA pulse. However, the time delays $\Delta\tau_0$ of the DLA pulses that were chosen by us in order to maximize the DLA energy gain A_L , are such that the standard trapping condition [17, 43, 44, 56] can only be satisfied for those electrons that are produced by the pump pulse.

3.1. Single color parallel polarization LWDA (SP-LWDA)

Below we describe the results of the PIC simulations of the SP-LWDA regime. Laser parameters are shown in the ‘SP’ column of table 1, and the time delays between the pump and DLA pulses are chosen to be in the proximity of $\Delta\tau = 24 \text{ fs}$. Such time delay, corresponding to constructive interference between the pump and DLA pulses, results in the optimal DLA regime, i.e. the largest number of injected electrons undergoing DLA, and reaching the highest energy. At moderate laser intensities, which are the focus of this paper, the complete blowout regime is not reached during the injection stage ($x \leq 100 \mu\text{m}$), and the plasma bubble is formed later. Therefore, the injected electrons are trapped into the potential well formed by the nonlinear plasma wave. Relativistic self-focusing of the pump laser pulse leads to the formation of the plasma bubble at the propagation distance $x \approx 200 \mu\text{m}$. Trapped electrons are accelerated in the plasma bubble, eventually reaching its center at the dephasing distance $x \approx 640 \mu\text{m}$, see figure 3(a). The spectrum of the accelerated electrons shown in figure 3(b) exhibits the distinctive double-

Table 1. Simulation parameters.

Parameter	SP	SO	TP
Laser wavelengths (μm): $\lambda_{\text{pump}}, \lambda_{\text{DLA}}$	0.8, 0.8	0.8, 0.8	0.8, 0.4
Polarization:	Parallel	Orthogonal	Parallel
Time delay ^a (fs): $\Delta\tau_0$	24	21	24
Pulse durations (fs): $\tau_{\text{pump}}, \tau_{\text{DLA}}$	20, 10	20, 10	20, 10
Spot size (μm): $w_{\text{pump}}, w_{\text{DLA}}$	10, 10.6	10, 10.6	10, 5.3
PIC cell size: $\Delta x/\lambda_{\text{pump}}, \Delta z/\lambda_p$	0.02, 0.02	0.02, 0.02	0.01, 0.02
Particles per cell: N_{cell}	8	8	8

^a Time delay is measured from the center of pump pulse to the center of DLA pulse.

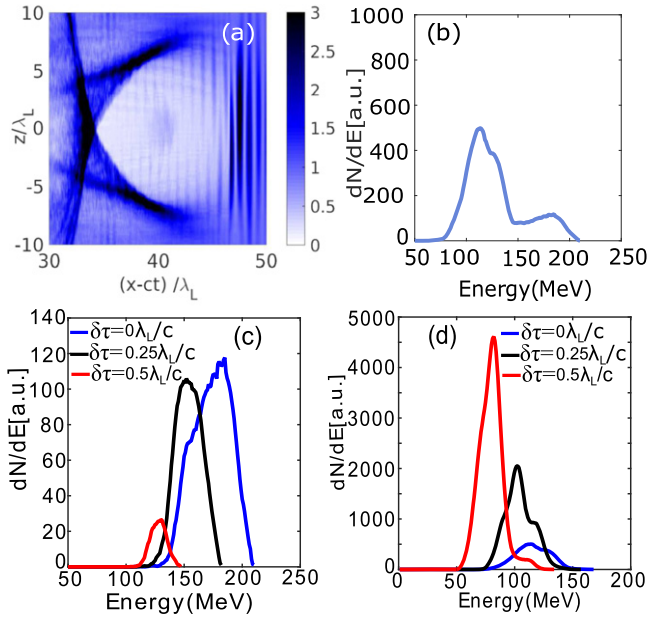


Figure 3. Acceleration of trapped electrons in the SP-LWDA regime. (a) Electron density and (b) spectrum of the accelerated electrons at $x = 640 \mu\text{m}$ for the time delay $\Delta\tau_0 = 24$ fs. (c) Spectra of the DLA ($A_L \geq 75$ MeV) and (d) non-DLA ($A_L < 75$ MeV) electrons for different time delay between pump and DLA laser pulses $\Delta\tau = \Delta\tau_0 + \delta\tau$: $\delta\tau = 0$ (blue), $\delta\tau = 0.25\lambda_L/c$ (black), and $\delta\tau = 0.5\lambda_L/c$ (red).

peaked energy distribution [16, 17], with the higher energy peak corresponding to the DLA population. The DLA electrons gain approximately 60 MeV more energy than the non-DLA electrons, thus forming an additional energy spectrum peak at $\gamma^{\text{DLA}}m_e c^2 \approx 170$ MeV.

Thus, we observe that, for the optimal pulse delay, the dynamics of injected electrons and their spatial distribution are quite similar to those discussed in [16, 17] for much higher power laser pulses. However, the spectrum of the accelerated electrons undergoes a dramatic change when the time delay $\Delta\tau$ deviates from the optimal one. Therefore, the time delay of the second DLA pulse becomes one of the crucial parameters in the moderate-intensity SP-LWDA regime. This sensitivity to $\Delta\tau$ is due to the small size of the plasma bubble: it can be seen from figure 3(a) that the plasma bubble in the moderate laser power regime is relatively small [60]: $R \sim \sqrt{a_0}/k_p \sim 5\lambda_L$. Therefore, the interference

between the overlapping pump and DLA pulses must be taken into account.

The sensitivity of the SP-LWDA regime to the time delay between the pulses is demonstrated by figures 3(c), (d) in which we compare spectra of DLA and non-DLA electrons for different values of $\Delta\tau \equiv \Delta\tau_0 + \delta\tau$, where $\Delta\tau_0 = 24$ fs, and $\delta\tau = 0$, $\lambda_L/4c$, $\lambda_L/2c$ is the variable time delay. Note that rigorously separating the DLA and non-DLA particles is not feasible because of the significant overlap between two spectra. This overlap can be clearly appreciated from figure 3(b). Therefore, we drew a boundary between them in a somewhat arbitrary way using $A_L \geq 75$ MeV as the cutoff for DLA-accelerated electrons. The resulting distribution functions between the DLA and non-DLA electrons were not significantly modified by changing this cutoff energy by 10 percent in either direction.

The variable time delay $\delta\tau = 0$ corresponds to the constructive interference between the DLA and pump pulses. The interference eventually becomes destructive when the variable time delay increases. To understand why the value of the time delay significantly affects the number and energy of the accelerated electrons, we observe that the combined laser intensity E_{\perp}^2 at the back of the bubble is highly sensitive to $\Delta\tau$. This can be observed by comparing E_{\perp}^2 at different $\Delta\tau$ in figures 2(b). Of particular importance is the combined lasers' intensity at the back of the bubble because it affects the bubble's shape and its ability to trap electrons. This effect is particularly important during the injection stage (dark region in 2(a)) because the potential well of the nonlinear plasma wave is still shallow at the plasma entrance.

Therefore, the destructive interference (e.g., for $\delta\tau = \lambda_L/2c$) drastically increases the total number of the trapped electrons, but results in a smaller number of the DLA electrons. Moreover, the energy gain of non-DLA electrons is also decreased by the destructive interference because of the reduction of the plasma bubble's accelerating field due to the beam loading effect [16, 61, 62]. An even more drastic reduction of the energy of the DLA electrons is caused by the simultaneous reductions of the energy gains from the laser and from the wake.

Thus, we observe that even sub-femtosecond ($\lambda_L/4c \approx 0.7$ fs) variations of the DLA/pump pulse delays causes significant performance deterioration in the SP-LWDA regime. The fact that the number of DLA electrons increases in the case of constructive interference ($\delta\tau = 0$) despite the

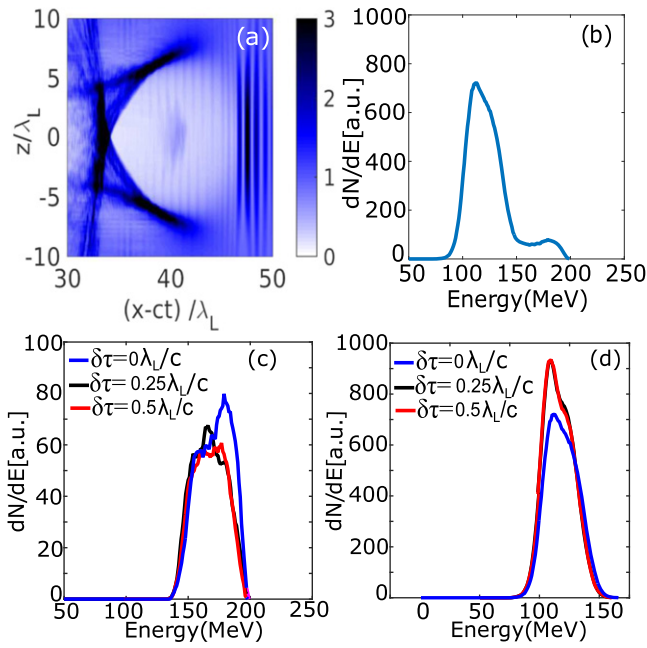


Figure 4. Acceleration of trapped electrons in SO-LWDA regime. (a) Electron density and (b) spectrum of accelerated electrons at $x = 640 \mu\text{m}$ for the time delay $\Delta\tau_0 = 21 \text{ fs}$. (c) Spectra of the DLA electrons and (d) non-DLA electrons for different time delays between the pump and DLA laser pulses $\delta\tau = \Delta\tau_0 + \delta\tau$: $\delta\tau = 0$ (blue), $\delta\tau = 0.25\lambda_L/c$ (black), and $\delta\tau = 0.5\lambda_L/c$ (red).

overall reduction of the number of the trapped electrons is consistent with one of the key results of the single-particle model described in section 2: the fraction of the DLA electrons increases with an increase of the laser electric field. The sensitivity of the LWDA mechanism to the time delay of the DLA pulse in the moderate laser power regime can be overcome by using different laser formats: SO-LWDA or TP-LWDA as described below.

3.2. Single color orthogonal polarization LWDA (SO-LWDA)

As was observed in section 3.1, the interference between the pump and DLA pulses can cause time jitter of the LWDA performance if the time delay $\Delta\tau$ between the pulses cannot be adequately controlled. A natural way to avoid the interference is to use two laser pulses with orthogonal polarizations: the SO-LWDA format. We investigate SO-LWDA scenario by leaving polarization of the DLA pulse in z direction and assuming the pump pulse is polarized in the y direction (which is perpendicular to the simulation plane $x-z$). The time delay $\Delta\tau_0 = 21 \text{ fs}$ between the pump and DLA pulses results in the optimal DLA regime in this scenario, i.e. the largest number of injected electrons undergoing DLA, and reaching the highest energy. The other laser and plasma parameters are the same as in the SP-LWDA scenario.

As observed from figure 4(a), the plasma bubble structure does not show any qualitative differences from the one in figure 3(a). And the spectra of trapped electrons for the optimal time delays are in general similar in the both SP-LWDA and SO-LWDA cases, see figures 4(b) and 3(b).

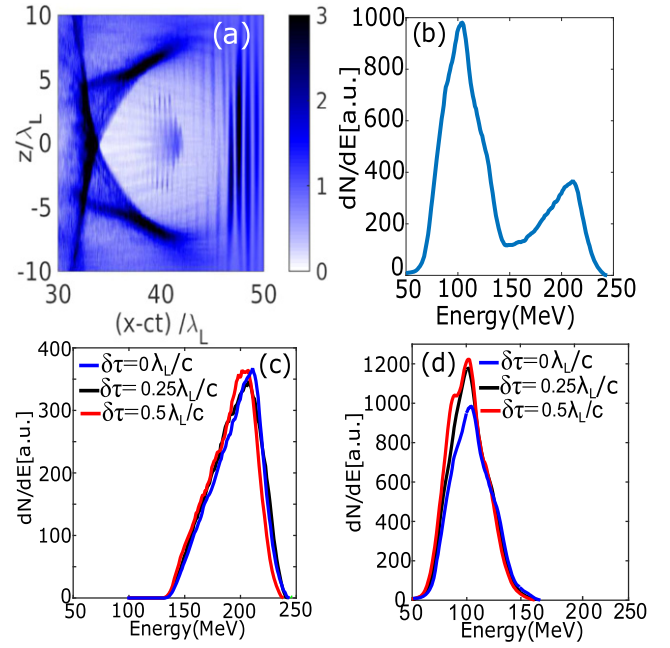


Figure 5. Electron acceleration in the TP-LWDA regime. (a) Electron density and (b) the spectrum of the accelerated electrons at $x = 640 \mu\text{m}$ for the time delay $\Delta\tau_0 = 24 \text{ fs}$. Energy spectra of the (c) DLA and (d) non-DLA electrons for different time delays $\Delta\tau = \Delta\tau_0 + \delta\tau$ between the pump and the DLA laser pulses: $\delta\tau = 0$ (blue), $\delta\tau = 0.25\lambda_L/c$ (black), and $\delta\tau = 0.5\lambda_L/c$ (red).

Similarly to the SP-LWDA case ($\delta\tau = 0$: constructive interference), the non-DLA electrons peaks at the energy $\gamma^{\text{non-DLA}} m_e c^2 \approx 110 \text{ MeV}$, and the DLA electrons peaks at $\gamma^{\text{DLA}} m_e c^2 \approx 170 \text{ MeV}$. The main difference is in the number of DLA electrons: it is somewhat smaller in the SO-LWDA scenario because it does not benefit from the constructive interference effects that are manifest in the SP-LWDA scenario.

As one can see from the comparison between figures 4(c), (d) and 3(c), (d), the variations in the DLA and the non-DLA spectra at different time delays are much smaller in the SO-LWDA scenario than in the SP-LWDA scenario. However, it is also clear that the best-performance numbers of the DLA and non-DLA electrons in the orthogonal polarization case are not as good as in the parallel polarization case. Therefore, we now consider an alternative approach to suppressing the interference: using different laser frequencies for the pump and DLA pulses.

3.3. Two-color parallel polarization LWDA (TP-LWDA)

Using two laser pulses with orthogonal polarizations, we improved the stability of the LWDA's performance with respect to the jitter of the delay time between the two laser pulses. The performance can be further improved by introducing a frequency-doubled ($\lambda_{\text{DLA}} = 0.5\lambda_{\text{pump}}$) DLA pulse. As noted above, we keep the normalized vector potential a_{DLA} and the power P_{DLA} of the DLA laser pulses the same as in the single-color cases. Therefore, the bubble structure in the TP-LWDA case is very similar to the one in SP-LWDA and SO-LWDA cases (see figure 5(a)).

One important advantage of the two-color scheme over the other two (single-color) approaches is that, according to figure 5(b), the number of DLA electrons is considerably higher. Remarkably, the fraction of the DLA electrons is close to $\eta_{\text{DLA}} \approx 35\%$ of the number of the non-DLA electrons for the optimal time delay ($\delta\tau = 0$) of the TP-LWDA scheme. This is considerably higher than the corresponding $\eta_{\text{DLA}} \approx 20\%$ for the optimal SP-LWDA format, or $\eta_{\text{DLA}} \approx 12\%$ for the optimal SO-LWDA format. In addition, the energy peak of the DLA electrons ($\gamma^{\text{DLA}} m_e c^2 \approx 210$ MeV) is almost twice of the energy peak of the non-DLA electrons, and is by 50 MeV higher than in the SP-LWDA and SO-LWDA scenarios. Remarkably, this energy increase is achieved without broadening the beam's energy spread.

The physical reason for the high performance of the TP-LWDA scheme harkens back to the results of the single-particle simulations reviewed in section 2: larger DLA laser fields result in a larger fraction of DLA electrons, and in their higher energy. By focusing the same power P_{DLA} into a smaller spot so as to maintain the same vector potential as in the single-color schemes, we can achieve larger electric field \mathbf{E}_\perp in the two-color scheme. And, because of the λ_{DLA}^2 scaling of the ponderomotive potential, the increase of the laser intensity is not accompanied by the distortion of the bubble. Additionally, relativistic guiding of the short-wavelength DLA pulse is not jeopardized by the $P_{\text{crit}} \approx 16.2(\lambda_p/\lambda_{\text{DLA}})^2$ GW scaling of the relativistic self-focusing threshold because the DLA pulse is guided by the pump-generated bubble.

While higher energy gain and charge yield represent important advantages of the TP-LWDA approach, we also expect a stable operation of this scheme because the interference between the pump laser pulse and the frequency doubled DLA laser pulse does not play an important role. The low sensitivity to the time delay $\Delta\tau$, which is a consequence of the lack of interference between the pump and DLA laser pulses, is illustrated by figures 5(c), (d). In contrast to the SP-LWDA scheme, we do not observe drastically different spectra of either DLA or non-DLA electrons if the time delay is changed from its optimal value.

4. Emission of x-ray radiation

Finally, we demonstrate a recently emerged important application for the electrons accelerated by the combination of the LWFA and DLA mechanisms: a DLA-assisted betatron radiation [20, 23]. While DLA-assisted radiation has been experimentally demonstrated by several groups [26, 63], the possibility of using a separate DLA frequency-doubled laser pulse for enhanced betatron radiation has not yet been described. Due to the large energy of transverse oscillations, DLA electrons are expected to emit copious x-rays. We demonstrate this by computing the synchrotron radiation from two representative electrons belonging to DLA and non-DLA groups of particles accelerated using the TP-LWDA scheme. The energies and transverse momenta of two such representative electrons are plotted in figures 6(a), (b),

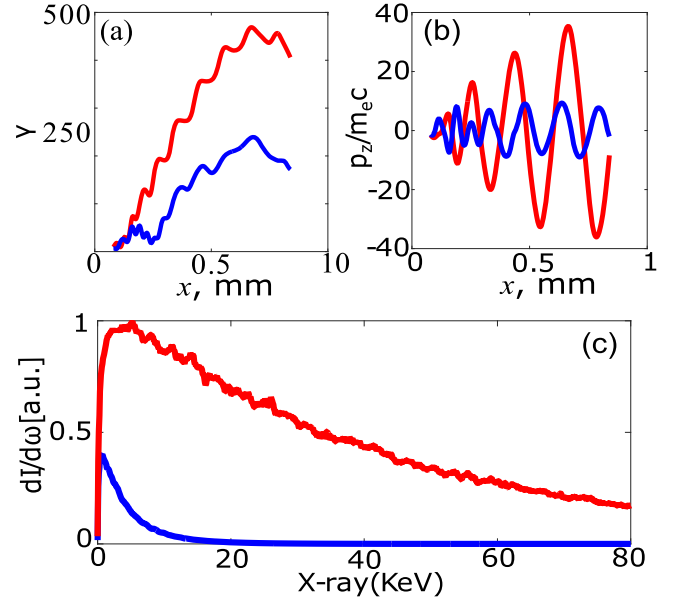


Figure 6. (a) The relativistic factor γ and (b) transverse momentum p_z for the representative DLA electron (red) and non-DLA electron (blue) as a function of the propagation distance x in TP-LWDA regime. (c) X-ray spectra for the electrons in (a) and (b). Laser and plasma parameters: table 1. Time delay: $\delta\tau = 0$.

respectively. It can be observed that a typical DLA electron has a larger relativistic factor γ and a larger transverse momentum p_z than a typical accelerated non-DLA electron. Specifically, $\gamma_{\text{max}}^{\text{DLA}} \approx 450$ and $p_{z,\text{max}}^{\text{DLA}} \approx 35m_e c$ for the DLA electron should be compared with $\gamma_{\text{max}}^{\text{n-DLA}} \approx 250$ and $p_{z,\text{max}}^{\text{n-DLA}} \approx 8m_e c$ for the non-DLA electron.

We can use these quantities to evaluate the critical frequency [64] which determines the frequency range of the emitted betatron radiation:

$$\omega_c = \frac{3}{2} \gamma^3 \frac{c}{\rho} \approx \frac{3\omega_p}{\sqrt{8}} \gamma^{3/2} \frac{p_z}{mc}, \quad (5)$$

We find from this formula that the DLA particle emits x-rays in a much wider energy range ($\omega_c^{\text{DLA}} \sim 45$ KeV) than the non-DLA particle ($\omega_c^{\text{n-DLA}} \sim 5$ KeV). One can readily check that such a difference in the critical frequencies can be mostly attributed to the difference in transverse momenta and, to much smaller degree, to the difference in full relativistic factors.

We calculate the synchrotron radiation spectra by, first, performing an integral along the electrons' trajectories [64] according to

$$\frac{d^2 I}{d\omega d\Omega} = \frac{e^2}{4\pi^2 c} \left| \int_{-\infty}^{\infty} \frac{\mathbf{n} \times (\mathbf{n} - \boldsymbol{\beta}) \times \dot{\boldsymbol{\beta}}}{(1 - \boldsymbol{\beta} \cdot \mathbf{n})^2} e^{i\chi} dt \right|, \quad (6)$$

where \mathbf{n} is the unit vector in the direction of radiation emission, $\boldsymbol{\beta} = \mathbf{v}/c$, $\dot{\boldsymbol{\beta}} = d\boldsymbol{\beta}/dt$, and $\chi \equiv \omega(t - \mathbf{n} \cdot \mathbf{r}(t))$. Next, equation (4) is integrated over all emission angles. Figure 6(c) confirms that spectrum for DLA electron extends over a much wider range of x-ray energies than the spectrum for a non-DLA electron. Also we find from this figure that the DLA and non-DLA x-ray spectra roughly peak at the photon energy

~ 7 KeV and ~ 0.6 KeV, respectively. Thus, we find that strong interaction with laser leads to much larger emission of radiation by DLA electrons and much broader spectrum of the emitted x-rays.

5. Conclusion

In conclusion, we have investigated three possible scenarios of LWDA in the moderate laser power regime: SP-LWDA, SO-LWDA and TP-LWDA. The SP-LWDA scheme exhibits extreme sensitivity to the time delay between the pump and DLA pulses, resulting in a very large potential variability of the final electron spectrum and charge. This sensitivity is shown to be due to the interference between the pump and the DLA pulses. The SO-LWDA scheme has relatively better performance than the SP-LWDA since it eliminates the interference and improves the sensitivity to delay-time jitter. However, the DLA charge yield is not improved compared with the SP-LWDA case. Finally, the TP-LWDA scheme achieves higher energy and larger charge of DLA electrons compared with the SP-LWDA and SO-LWDA. Furthermore, the TP-LWDA increases the stability by lowering the requirement for synchronization between the pump pulse and the DLA pulse. With the introduction of the higher frequency DLA pulse, the hybrid laser wakefield and direct laser plasma accelerator may become even more promising for future applications, especially for novel x-ray radiation sources.

Acknowledgments

This work was supported by DOE grants DE-SC0007889 and DE-SC0010622, and by an AFOSR grant FA9550-16-1-0013. The authors thank the Texas Advanced Computing Center for providing HPC resources.

ORCID iDs

T Wang  <https://orcid.org/0000-0002-5934-8031>

References

- [1] Tajima T and Dawson J 1979 *Phys. Rev. Lett.* **43** 267
- [2] Faure J, Glinec Y, Pukhov A, Kiselev S, Gordienko S, Lefebvre E, Rousseau J, Burgy F and Malka V 2004 *Nature* **431** 54
- [3] Geddes C, Toth C, Van Tilborg J, Esarey E, Schroeder C, Bruhwiler D, Nieter C, Cary J and Leemans W 2004 *Nature* **431** 538
- [4] Mangles S *et al* 2004 *Nature* **431** 535
- [5] Leemans W, Nagler B, Gonsalves A, Toth C, Nakamura K, Geddes C, Esarey E, Schroeder C and Hooker S 2006 *Nat. Phys.* **2** 696
- [6] Leemans W *et al* 2014 *Phys. Rev. Lett.* **113** 245002
- [7] Wang X *et al* 2013 *Nat. Commun.* **4** 1988
- [8] Kim H T, Pae K H, Cha H J, Kim I J, Yu T J, Sung J H, Lee S K, Jeong T M and Lee J 2013 *Phys. Rev. Lett.* **111** 165002
- [9] Steinke S *et al* 2016 *Nature* **530** 190
- [10] Pukhov A and Meyer-Ter-Vehn J 2002 *Appl. Phys. B* **74** 355–61
- [11] Li Z, Tsai H-E, Zhang X, Pai C-H, Chang Y-Y, Zgadzaj R, Wang X, Khudik V, Shvets G and Downer M C 2014 *Phys. Rev. Lett.* **113** 085001
- [12] Pukhov A, Sheng Z-M and Meyer-ter-Vehn J 1999 *Phys. Plasmas* **6** 2847
- [13] Gahn C, Tsakiris G D, Pukhov A, Meyer-ter-Vehn J, Pretzler G, Thirolf P, Habs D and Witte K J 1999 *Phys. Rev. Lett.* **83** 23
- [14] Khudik V N, Zhang X, Wang T and Shvets G 2018 *Phys. Plasmas* **25** 083101
- [15] Khudik V N, Arefiev A V, Zhang X and Shvets G 2016 *Phys. Plasmas* **23** 103108
- [16] Zhang X, Khudik V N and Shvets G 2015 *Phys. Rev. Lett.* **114** 184801
- [17] Zhang X, Khudik V N, Pukhov A and Shvets G 2016 *Plasma Phys. Control. Fusion* **58** 034011
- [18] González I G, Ekerfelt H, Hansson M, Audet T L, Aurand B, Desforges F G and Duffrénoy S D 2018 Effects of the dopant concentration in laser wakefield and direct laser acceleration of electrons *New J. Phys.* **20** 053011
- [19] Shaw J L, Lemos N, Marsh K A, Froula D H and Joshi C 2018 Experimental signatures of direct-laser-acceleration-assisted laser wakefield acceleration *Plasma Phys. Control. Fusion* **60** 044012
- [20] Shaw J L 2016 *PhD Thesis* University of California Los Angeles
- [21] Shaw J L, Lemos N, Amorim L D, Vafaei-Najafabadi N, Marsh K A, Tsung F S, Mori W B and Joshi C 2017 Role of direct laser acceleration of electrons in a laser wakefield accelerator with ionization injection *Phys. Rev. Lett.* **118** 064801
- [22] Shaw J L, Lemos N, Marsh K A, Tsung F S, Mori W B and Joshi C 2016 Estimation of direct laser acceleration in laser wakefield accelerators using particle-in-cell simulations *Plasma Phys. Control. Fusion* **58** 034008
- [23] Lemos N, Martins J L, Tsung F S, Shaw J L, Marsh K A, Albert F, Pollock B B and Joshi C 2016 Self-modulated laser wakefield accelerators as x-ray sources *Plasma Phys. Control. Fusion* **58** 034018
- [24] Adachi M, Miura E, Kato S, Koyama K, Masuda S, Watanabe T, Okamoto H, Ogata A and Tanimoto M 2006 Cascade acceleration of electrons by laser wakefield and direct laser field *Japan. J. Appl. Phys.* **45** 4214
- [25] Nemeth K, Shen B, Li Y, Shang H, Crowell R, Harkay K C and Cary J R 2007 *Phys. Rev. Lett.* **100** 095002
- [26] Cipiccia S *et al* 2011 *Nat. Phys.* **7** 867
- [27] Nam I, Hur M S, Uhm H S, Hafz N A M and Suk H 2011 *Phys. Plasmas* **18** 043107
- [28] Corde S, Ta Phuoc K, Fitour R, Faure J, Tafzi A, Goddet J P, Malka V and Rousse A 2011 *Phys. Rev. Lett.* **107** 255003
- [29] Ta Phuoc K, Esarey E, Leurent V, Cormier-Michel E, Geddes C G R, Schroeder C B, Rousse A and Leemans W P 2008 *Phys. Plasmas* **15** 063102
- [30] Phuoc K T, Corde S, Fitour R, Shah R, Albert F, Rousseau J-P, Burgy F, Rousse A, Seredov V and Pukhov A 2008 *Phys. Plasmas* **15** 073106
- [31] Shaw J L, Tsung F S, Vafaei-Najafabadi N, Marsh K A, Lemos N, Mori W B and Joshi C 2014 *Plasma Phys. Control. Fusion* **56** 084006
- [32] Cole J M *et al* 2015 Laser-wakefield accelerators as hard x-ray sources for 3D medical imaging of human bone *Sci. Rep.* **5** 13244

- [33] Kneip S *et al* 2010 Bright spatially coherent synchrotron x-rays from a table-top source *Nat. Phys.* **6** 980
- [34] Kneip S *et al* 2011 X-ray phase contrast imaging of biological specimens with femtosecond pulses of betatron radiation from a compact laser plasma wakefield accelerator *Appl. Phys. Lett.* **99** 093701
- [35] Fourmaux S *et al* 2011 Single shot phase contrast imaging using laser-produced Betatron x-ray beams *Opt. Lett.* **36** 2426–8
- [36] Zhao T Z *et al* 2016 High-flux femtosecond x-ray emission from controlled generation of annular electron beams in a laser wakefield accelerator *Phys. Rev. Lett.* **117** 094801
- [37] Chen M, Sheng Z, Ma Y and Zhang J 2006 Electron injection and trapping in a laser wakefield by field ionization to high-charge states of gases *J. Appl. Phys.* **99** 056109
- [38] Pak A, Marsh K A, Martins S F, Lu W, Mori W B and Joshi C 2010 Injection and trapping of tunnel-ionized electrons into laser-produced wakes *Phys. Rev. Lett.* **104** 025003
- [39] Tsai H-E *et al* 2015 *Phys. Plasmas* **22** 023106
- [40] Malka G *et al* 2002 *Phys. Rev. E* **66** 066402
- [41] Nakamura K, Nagler B, Tóth C, Geddes C G R, Schroeder C B, Esarey E and Leemans W P 2007 *Phys. Plasmas* **14** 056708
- [42] Dong P *et al* 2010 *Phys. Rev. Lett.* **104** 134801
- [43] Xu X L *et al* 2010 *Phys. Rev. Spec. Top. Accel. Beams* **17** 061301
- [44] Schroeder C B, Vay J-L, Esarey E, Bulanov S S, Benedetti C, Yu L-L, Chen M, Geddes C G R and Leemans W P 2010 *Phys. Rev. Spec. Top. Accel. Beams* **17** 101301
- [45] Yu L-L, Esarey E, Schroeder C B, Vay J-L, Benedetti C, Geddes C G R, Chen M and Leemans W P 2014 *Phys. Rev. Lett.* **112** 125001
- [46] Kostyukov I, Pukhov A and Kiselev S 2004 *Phys. Plasmas* **11** 11
- [47] Huang T W, Zhou C T, Robinson A P L, Qiao B, Arefiev A V, Norreys P A, He X T and Ruan S C 2017 Nonlinear parametric resonance of relativistic electrons with a linearly polarized laser pulse in a plasma channel *Phys. Plasmas* **24** 043105
- [48] Pukhov A 1999 *J. Plasma Phys.* **61** 425
- [49] Ammosov M V, Delone N B and Krainov V P 1986 *Sov. Phys. —JETP* **64** 1191
- [50] Chen M, Cormier-Michel E, Geddes C G R, Bruhwiler D L, Yu L L, Esarey E, Schroeder C B and Leemans W P 2012 *J. Comput. Phys.* **236** 220
- [51] Karmakar A and Pukhov A 2007 *Laser Part. Beams* **25** 371
- [52] Pollock B B *et al* 2011 *Phys. Rev. Lett.* **107** 045001
- [53] Vargas M *et al* 2014 *Appl. Phys. Lett.* **104** 231108
- [54] Schmida K and Veisz L 2012 *Rev. Sci. Instrum.* **83** 053304
- [55] Jolly S W, He Z, McGuffey C, Schumaker W, Krushelnick K and Thomas A G R 2012 *Rev. Sci. Instrum.* **83** 073503
- [56] Pak A, Marsh K A, Martins S F, Lu W, Mori W B and Joshi C 2010 *Phys. Rev. Lett.* **104** 025003
- [57] Liu J S *et al* 2011 *Phys. Rev. Lett.* **107** 035001
- [58] McGuffey C *et al* 2010 *Phys. Rev. Lett.* **104** 025004
- [59] Chen M, Esarey E, Schroeder C B, Geddes C G R and Leemans W P 2012 *Phys. Plasmas* **19** 033101
- [60] Gordienko S and Pukhov A 2005 *Phys. Plasmas* **12** 043109
- [61] Tsung F S, Narang R, Mori W B, Joshi C, Fonseca R A and Silva L O 2004 *Phys. Rev. Lett.* **93** 185002
- [62] Tzoufras M, Lu W, Tsung F S, Huang C, Mori W B, Katsouleas T, Vieira J, Fonseca R A and Silva L O 2008 *Phys. Rev. Lett.* **101** 145002
- [63] Lemos N *et al* 2018 Bremsstrahlung hard x-ray source driven by an electron beam from a self-modulated laser wakefield accelerator *Plasma Phys. Control. Fusion* **60** 054008
- [64] Jackson J D 2011 *Classical Electrodynamics* 3rd edn (New York: Wiley) 2001